frontiers

Supplementary Material

SI 1. Supplementary discussion: Regional climate and environmental change

Whereas many aspects of past palaeoclimatic change reflect orbital parameters, with changing amounts of energy from the sun reaching the earth, the 4.2 ka event seems to rather reflect changes in circulation patterns within and between regions of the earth (e.g. Bini et al., 2019). Given the similar climatic and orbital conditions to the present day, the 4.2 ka event is also particularly interesting in light of contemporary concerns about future climate change.

Given the limitations of the Maltese palaeoenvironmental archives – with their taphonomic biases, chronological uncertainties, and problems of separating anthropogenic and climatic signals – we now turn to evaluate the wider regional climatic situation to cast light on what may have transpired in Malta around 4.2 ka. Given the lack of high-resolution and long-term records for the Maltese islands, we use climate data from a neighbouring area (Italy) to conduct modelling of Maltese archaeological data. It is therefore important to justify the relevance of these data to Malta

Sicily is close (~100 km) to the Maltese Islands and much more palaeoclimate and palaeoecological data is available. However, in many cases the dating resolution is still relatively coarse. Some key records come from pollen assemblages from lake cores. Firstly, some of the same problems influence these records, such as it not being clear what explains significant differences between assemblages and the difficulty in separating anthropogenic and climate signals.

Tinner and colleagues (2009) report the site of Gorgo Basso in western Sicily. Interesting here is that tree pollen shows a pronounced drop from about 4.5 ka. This decline, however, was two-stage, with an initial low at 4.3-4.2 ka, followed by a rise, and then another low ~3.9 ka. A similar pattern comes from the pattern of arboreal pollen. Quercus, for instance, rose steeply from around 5.5 ka, stayed high until about 4.7 ka, and then fell to a low point at about 3.9 ka. Synchronously, the highest level of Pistacia was recorded about 3.9 ka. Calò and colleagues (2012) present pollen data for Lago Preola in western Sicily. Interestingly here we can see a basic theme; in the second half of the third millennium BC many records show broadly similar patterns, but there are variations in the specifics. At Preola, we can for instance see a rise in tree pollen from about 7 ka, a phase of reduced tree pollen begins around just before 5 ka, falling to two low points and ~4.5 and 3.4 ka separated by a partial rise ~3.9 ka.

In southern Sicily, the Biviere di Gela shows declining tree pollen from about 5.5 ka, reaching a low point around 4.2 ka and then staying low for another 500 years or so (Noti et al., 2009). When specifically wetland and aquatic pollen are considered, this low point in trees around 4.2 ka, matched by a spike in herb pollen, stands out more.

These changes seem to mirror changes across adjacent areas of the Mediterranean more broadly (Roberts et al., 2019). Di Rita and Magri (2019) situate these changes in terms of the progressive northward movement of the North African High Pressure cell.

Given the complexities of pollen records, we next looked to mainland Italy for high resolution palaeoclimate records. While now moving further from Malta, we nevertheless see Italian records are offering reasonable proxies for the palaeoclimate of the central Mediterranean. Speleothem records have the benefit of precise uranium series age estimates and multiple isotope measurements. Oxygen isotopes primarily reflect changes in rainfall (i.e. higher $\delta^{18}O$ values indicate aridity). $\delta^{13}C$ values largely reflect biological activity in soil, so lower rainfall means reduced biological activity in soil and increasing $\delta^{13}C$ values. Different sites have different strengths and weaknesses in terms of their data. For instance, Corchia Cave has produced an important record (Isola et al., 2019), but is a large and deep cave at a relatively high altitude, with complex 'plumbing'. We therefore selected the Rennella Cave record for our analysis as discussed below. We mention in passing the complexity of available data; with the Corchia record presented by Isola and colleagues (2019) suggesting aridity some centuries earlier that at Renella.. The meaning of this intra- and inter-site variability is currently unclear, and should be kept in mind when considering the definition and timing of the 4.2 ka event.

Renella Cave provides a record of oxygen and carbon isotope variability covering most of the Holocene (Drysdale et al., 2006; Zanchetta et al., 2016). Both isotopes show high variability through time, but it is possible to describe general trends. Both indicate decreasing aridity in the millennium from ca. 5.8 to 4.8 ka (our discussion here focusses on the Zanchetta et al. 2016 paper, with its higher resolution data). So, climate was relatively humid around 4.8 ka. It can be noted in passing that this climate peak correlates with the revised timing on the origin of the Tarxien period in Malta, as discussed in the main text. After about 4.8 ka both oxygen and carbon isotopes demonstrate aridifying climate. Both isotopes show less negative values (i.e. drier conditions) at ~4.25 ka followed by a slight rise in values and then to even less negative values ~4 ka, although of course discussion of such precise ages depends on the accuracy of the age-depth model. For both isotopes these are the most negative values in a long span of time – and what is also interesting is that while other periods show some similarly negative values they are close in time to also considerably higher values. It is only in the ~4.4 to 3.8 ka range there are no high points – so aridity is indicated both in direct terms by less negative isotope signals, but also by the reduction in fluctuation. In this view then, the '4.2 ka event' actually seems to reflect several centuries of arid conditions, between ~4.4 and 3.8 ka, with particular arid points at 4.25 ka and (even more arid) at about or slightly after 4 ka. We use the Renella Cave data for our REC model analyses described in the main text and in SI 3.

SI.2 Supplementary discussion: Xagħra Circle Broken Statue Chronological Model

Fragments of the broken statue were found across a narrow vertical range (supplementary table 2). We compared four chronological models for the radiocarbon dates from contexts in which pieces of the broken statue were found. The models differed in terms of the boundaries we specified for the start and end of the statue deposition process – these boundaries constitute the priors in Bayesian chronological models. In OxCal, there are several different temporal boundary types that can be specified for a group of sample dates (Bronk Ramsey 2009). The three we used are called "Boundary", "Sigma", and "Tau" boundaries. The "Boundary" type implies that the given

depositional process had abrupt start and/or end dates. The "Sigma" type implies a more gradual increase and/or decrease in the temporal distribution of radiocarbon samples with the slopes like the tails of a normal (Gaussian) distribution. Finally, the "Tau" boundary implies an exponential increase/decrease in the temporal density of samples through time with very long, gradual tails.

These boundaries can be combined in different ways to produce an assortment of potential models (Bronk Ramsey 2009). Not all combinations are allowed, however, and only a couple were of use to us for evaluating the possibility that the statue pieces were deposited in a single break-and-scatter process. The first model we created involved two uniform boundaries. This model implied that the deposition of the statue pieces (or, more specifically, the associated radiocarbon samples) started and ended abruptly. The second model involved an initial Sigma and terminal uniform boundary, which would imply that there was a somewhat gradual accretion of samples leading to an abrupt end of the deposition process. The third model involved a Tau boundary and a uniform boundary, implying a few early associations between radiocarbon samples and statue pieces followed by a much more rapid accumulation of samples and then finally an abrupt end to the process. The last model involved two Sigma boundaries. This model implied that the sample-statue associations had a normal distribution in time with no abrupt boundaries, which would indicate that the statue pieces continued to be part of an active deposition process for some time after their initial breaking/scattering. No other combinations were allowed by OxCal.

We reasoned that the first three of these models would be congruent with the idea that the statue was broken, scattered, and then reasonably stationary with the final temporal associations indicated by the date of a terminal uniform boundary.

To compare the models, we used OxCal's model fit statistics. The key statistic is called the "Agreement Index" (Bronk Ramsey 1995, 2009). It indicates the degree to which "unmodelled" calibrated date distributions overlap with their respective "modelled" distributions. A given date distribution is referred to as "unmodelled" after calibration but before any Bayesian priors have been applied while it is referred to as "modelled" afterward. The Bayesian modelling process can be thought of as reshaping calibrated date distributions to reflect prior knowledge about the temporal location of the samples in question. OxCal's agreement index essentially measures the magnitude of these adjustments. Given a single date density, for example, the agreement index would be high if the constraints imposed by the model priors (e.g., the group boundaries described above) had only a slight effect on the shape and location of the date distribution. In contrast, if the unmodelled distributions are adjusted by a large amount, the agreement index would be lower. In effect, the index is reporting the degree to which the raw data "agree" with the Bayesian model. Very low agreement potentially indicates an empirical mis-match, suggesting that a given model may not sufficiently reflect the temporal distribution and chronological arrangement of the sample dates. Thus, the agreement index can be used to compare Bayesian models given a single set of dates under the assumption that one model outperforms another if the empirical observations agree more with the former than the latter.

Using the agreement index, we compared the four models described earlier (see supplementary table 3). The results indicated that the best performing model – the one with the highest agreement index – was the one with an initial "Tau" boundary followed by a terminal uniform boundary. This model implies that the group of samples contains some very early material, followed by an exponential rise

in temporal density of samples with an abrupt termination. A temporal distribution of samples like this could be explained in a few ways. In one scenario the statue was broken early on and a small number of radiocarbon samples (bones, to be specific) then entered into association with the broken statue pieces. As time progressed, more bones were deposited (and associated with the statue pieces), with the number of deposits/associations rising rapidly at the end of the process finally ceasing abruptly at a terminal boundary. In another scenario, some bones were deposited into their contexts early on. Then, the statue was broken near the terminal temporal boundary of the model while more bones were simultaneously making their way into the same depositional contexts creating the observed associations. Older samples – already in the cave at the time the statue was broken – could then have become associated with the statue pieces, or redeposited as a result of later mixing. The deposition of bones then ended abruptly at the terminal boundary. Finally, the statue breaking may have occurred at the terminal temporal boundary of the model. This last scenario would suggest that a few early radiocarbon samples entered into the cave followed by a rapid increase in sample deposition and then the statue was broken, entering into association with the bones at the same time that further bone deposition ceased.

A couple pieces of evidence allow us to eliminate the first potential scenario, we think. Firstly, the temporal distribution of sample associations implies that the bulk of associations between bones and statue pieces occurred close to the terminal temporal boundary of the model. In our view, the most parsimonious explanation is that the statue was broken either near or at the terminal boundary instead of having occurred earlier as the first scenario suggests. Secondly, the way the site was used and its stratigraphic character make it likely that there should be some cycling of older material into younger deposits. Had the statue been broken and deposited when the earliest bone samples were deposited, then, we would expect the radiocarbon sample associations to be more thoroughly mixed – i.e., less densely clustered toward the terminal boundary with more early associations. We would also expect more vertical spread of the statue fragments. With respect to the Bayesian models, that would have meant a more uniform or perhaps normal distribution of sample dates between the boundaries rather than one tightly clustered toward the terminal end with a fat early tail like the distribution we actually observed. Thus, we argue that the statue was probably broken toward the end of the bone deposition process and perhaps even occurred at the termination of that process.

SI.3. Supplementary discussion: REC Models

We used a radiocarbon-dated event-count (REC; Carleton, 2020) model to explore the relationship between Maltese radiocarbon-dated event counts and regional precipitation. The event-counts refer to the number of archaeological radiocarbon samples dated to a given time. These samples come from the published literature on the archaeology of Malta, including recent excavation work. The available dates are summarized in supplementary table 1. The precipitation amounts in our analyses were indicated by a $\delta^{18}O$ proxy record recovered from a flowstone archive in a central Italian cave. This $\delta^{18}O$ record was used as the sole covariate in our regression models. We aimed to test whether fluctuations in rainfall amount corresponded with through-time fluctuations in the abundance of radiocarbon-dated samples from Malta.

To begin we selected an appropriate temporal resolution and a target analytical interval. We settled on a 20-year resolution for the analysis and defined our temporal interval to begin at 3500 BC and end at 2730 BC. The resolution was selected as a compromise between three factors: the limited meaningful temporal resolution of radiocarbon dates; a temporal scale appropriate for discerning the impact of climate fluctuations on human lives and inter-generational social changes; and, lastly, computational limitations (higher resolutions correspond to large numbers of parameters in REC models that require estimation and, therefore, longer computation times). The time range we selected corresponds to the 4.2 ka event and the preceding centuries of the Temple Period.

REC models were developed to promote better handling of radiocarbon-date uncertainty in the context of dates-as-data analyses (Carleton 2020, Carleton and Groucutt 2020). These types of analyses involve treating through-time changes in the number of radiocarbon samples in archaeological deposits as a proxy for a target process of interest – usually human population size, but sometimes a more abstract target like human activity levels has been the focus instead. Each sample is thought to date an "event" of interest, like the founding or occupation of a habitation site, the use of a hearth, the death of an individual, etc. More such events in a given time/place is thought to be indicative of larger population sizes and/or more human activity broadly speaking. However, radiocarbon samples are only dated imprecisely, which means they have (often significant) amounts of chronological uncertainty. This uncertainty has to be accounted for when trying to estimate the number of corresponding events that occurred in a given interval (or sequence of intervals). Along similar lines, many of the potential covariates archaeologists wish to explore typically also contain chronological uncertainty. Paleoclimate records, for instance, are regularly compared to radiocarbon-date proxies and those climate records also contain significant chronological uncertainty that needs to be accounted for.

REC models attempt to grapple with this dating uncertainty for the purposes of statistical regression. The aim of the approach is to propagate the chronological uncertainty in the variable observations up to target regression model parameters---e.g., regression coefficients. In the REC models published so far, this uncertainty propagation has been accomplished by using hierarchical Bayesian regression (Carleton 2020, Stewart et al. 2021 and, for details about Bayesian hierarchical models, see Gelman and Hill 2007). In this context, the hierarchy refers to the arrangement of the parameters in the regression model, of which there are two levels. The bottom level is comprised of regression model parameters that refer to individual regression models, each involving a randomly drawn event-count sequence and one or more probable covariate sequences (e.g., a probable palaeoclimate record, given the chronological uncertainty in the relevant age-depth model). These lower-level regression models have regression coefficients that are thought to be drawn from a super-population. That super population is characterized by a set of hyper-parameters and those parameters constitute the upper level of the hierarchy in a REC model. The sample of probable lower-level regression models is used to estimate the hyper-parameters at the top of the hierarchy. The posterior distributions of these top-level parameters, then, ultimately reflect variation among the individual, randomly drawn independent and dependent variable sequences. Since variation among different probable sequences exists because of chronological uncertainty, the posterior distributions for the top-level parameters reflect that uncertainty. In other words, the chronological uncertainty is propagated into the target regression model parameters, which affects (usually increases) their variance as would be expected.

The propagation also reduces bias, again as expected, and importantly it means the final inferences from the model account for our uncertainty about sample dates.

While this approach has been demonstrated to work well in simulation, we decided to adapt it for this analysis. Ongoing research on REC models has revealed that biases in REC model regression parameters can be further reduced by taking a much larger sample of probable event-count sequences and corresponding covariate sequences. Unfortunately, the hierarchical approach employed previously with REC models is computationally inefficient for large samples (more than 100 or so probable dependent-independent variable combinations). Ideally, in order to propagate the chronological uncertainty of the individual calibrated date distributions up to the target parameters of the regression model, many more samples of probable event count sequences (and corresponding covariates) should be used, preferably tens to hundreds of thousands. With this in mind, we abandoned the hierarchical parameter arrangement and instead created a custom MCMC simulation that effectively draws a new set of variable sequences (dependent and independent variables) in each iteration of the MCMC. This approach reduces the total number of parameters that need to be estimated and allows for a much larger sample of probable variable sequences to be explored and accounted for – more of the observable chronological uncertainty in radiocarbon dates and age-depth models can be propagated up to the target regression model parameters.

Following Carleton (2020) and Stewart et al. (2021), we used a Negative-Binomial NB-REC model. The Negative-Binomial distribution is appropriate for count data and is commonly used instead of the simpler Poisson distribution in cases where observed data are over- or under-dispersed (i.e., have a higher or lower variance than the standard Poisson distribution of the same mean would predict) (Hilbe 2014). As has been argued elsewhere, over-/under-dispersion is an expected characteristic of radiocarbon-dated event count sequences because of the nature of chronological uncertainty and its impact on count data (Carleton 2020, Carleton and Groucutt 2020). Thus, the Negative-Binomial is a good choice for REC models. It has two parameters that together determine the location (mean) and scale (variance) of the distribution. These two parameters are commonly denoted ‘p’ and ‘r’, a convention followed in Carleton (2020). In an NB-REC model, the regression (the function relating covariates to the NB-distributed dependent event count variable) determines the ‘r’ parameter and the ‘p’ parameter is estimated from the data. Importantly, every observation in a given event count sequence is used to model a separate NB variable conditioned on the covariate(s), which means one ‘r’ parameter has to be estimated for every time interval in the sequence. So, for example, a 1000-year analytical interval at a decadal resolution implies 100 intervals and, therefore, 100 ‘r’ parameters to be estimated in addition to the other model parameters in the regression.

Using the adapted REC model setup, we created two NB-REC models. For one model, we compared event-count sequences based on all of the dates in the Maltese archaeological radiocarbon date database to the $\delta^{18}O$ record. In the other model, we compared only the dates from the Xagħra Circle, where the most detailed studies of a relevant period archaeological site have been conducted. The event-count sequences were created by sampling the relevant calibrated radiocarbon date densities with replacement many times. Each random draw was then collated into a single count series by counting the number of events dated to a given time, where the times are determined by a temporal grid. This grid was defined by the temporal resolution and span of interest, i.e., 3500–2730 BC with 20-year bins. We used annually sampled calibrated date densities calculated with the R package

"clam" (Blaauw 2021) to produce the necessary event-count samples. Along similar lines, the $\delta^{18}O$ record samples were produced by first creating ensembles of the relevant age-depth model in OxCal and then assigning time-stamps to the palaeoclimatic observations with those sampled age-depth models. The OxCal age-depth model was produced using OxCal's Poisson deposition model (Bronk Ramsey 2008, 2009) and was comparable to the published age-depth model for the flowstone data (see supplementary figure 1). Since the $\delta^{18}O$ data were available at an annual resolution, we used a smooth kernel density estimator to produce a running average $\delta^{18}O$ function sampled at the centers of the 20-year time bins used to produce the event-count samples. Effectively, this sampling strategy meant that we could compare 20-year event counts with correspondingly dated 20-year average $\delta^{18}O$ values.

As noted, the model parameters were estimated with MCMC (supplementary figure 2), specifically a Metropolis-Hasting algorithm with a Gibbs step for the Negative-Binomial 'p' parameter. The simulation was run for over 950,000 iterations from which the first 100,000 were discarded as burn-in. Some of those initial iterations were also used in an adaptive step to help determine the best proposal distributions for the model's parameters. The resulting MCMC chains for each parameter were then inspected for convergence visually and with the help of standard Geweke diagnostics (Geweke, 1992). Any parameter chains that exceeded a p-value of 0.001 in the Geweke tests were then visually inspected for convergence problems. All simulations and analyses were conducted in R (R Core Team 2021) with the help of several packages, including bigmemory (Kane et al. 2013), clam (Blauuw 2021), ggplot2 (Wickham 2016), and ggpubr (Kassambara 2020).

Supplementary references

Bini, M., Zanchetta, G., Perşoiu, A., Cartier, R., Català, Cacho, I. (2019), The 4.2 ka BP event in the Mediterranean region: an overview. *Clim. Past.* 15, 555-577. doi.org/10.5194/cp-15-555-2019

Blaauw, M. (2021). clam: Classical Age-Depth Modelling of Cores from Deposits. R package version 2.3.9. https://CRAN.R-project.org/package=clam

Bronk Ramsey, C. (1995). Radiocarbon Calibration and Analysis of Stratigraphy: The OxCal Program. *Radiocarbon*, *37*(2), 425–430.

Bronk Ramsey, C. (2008). Deposition models for chronological records. *Quaternary Science Reviews*, *27*(1–2), 42–60. https://doi.org/10.1016/j.quascirev.2007.01.019

Bronk Ramsey, C. (2009). Bayesian Analysis of Radiocarbon Dates. *Radiocarbon*, *51*(1), 337–360. https://doi.org/10.2458/azu_js_rc.v51i1.3494

Carleton, W. C. (2020). Evaluating Bayesian Radiocarbon-dated Event Count (REC) models for the study of long-term human and environmental processes. *Journal of Quaternary Science*, *36*(1), 110–123. https://doi.org/10.1002/jqs.3256

Carleton, W.C., Groucutt, H.S. (2020). Sum things are not what they seem: Problems with point-wise interpretations and quantitative analyses of proxies based on aggregated radiocarbon dates. *The Holocene* 31, 630-643. DOI: 10.1177/0959683620981700

Calò, C., Henne, P.D., Curry, B., Magny, M., Vescovi, E., La Mantia, T., et al. (2012). Spatio-temporal patterns of Holocene environmental change in southern Sicily. *Palaeogeog., Palaeoclim., Palaeoeco.* 323, 110-122. doi:10.1016/j.palaeo.2012.01.038

Di Rita, F., Magri, D. (2019). The 4.2 ka event in the vegetation record of the central Mediterranean. *Clim. Past* 15, 237-251. https://doi.org/10.5194/cp-15-237-2019

Drysdale, R.N., Zanchetta, G., Hellstrom, J., Maas, R., Fallick, A., et al. (2006). Late Holocene drought responsible for the collapse of Old World Civilisations is recorded in an Italian cave flowstone. *Geology* 34, 101-104. https://doi.org/10.1130/G22103.1

Gelman, A., & Hill, J. (2007). *Data Analysis Using Regression and Multilevel/Hierarchical Models*. Cambridge University Press.

Geweke, J. (1992). Evaluating the Accuracy of Sampling-Based Approachesto the Calculation of Posterior Moments. In J. M. Bernardo, J. O. Berger, A. P. Dawid, & A. F. M. Smith (Eds.), *Bayesian Stastistics* (4th ed., pp. 169–193). Clarendon Press.

Hilbe, J. M. (2014). *Modeling Count Data*. Cambridge University Press.

Isola, I., Zanchetta, G., Drysdale, R.N., Regattieri, E., Bini, M., Bajo, P., et al. (2019). The 4.2. ka event in the central Mediterranean: new data from a Corchia speleothem (Apuan Alps, central Italy). *Clim. Past.* 15, 135-151. https://doi.org/10.5194/cp-15-135-2019

Malone, C., Stoddart, S., Trump, D., Bonanno, A., Pace, A. (eds.) (2009), *Mortuary Ritual in Prehistoric Malta*. *The Brochtorff Circle Excavations (1987-1994)*. Cambridge, McDonald Institute for Archaeological Research.

Malone, C., Cutajar, N., McLaughlin, T.R., Mercieca-Spiteri, B., Pace, A., Power, R.K., et al. (2019), Island questions: The chronology of the Brochtorff Circle at Xagħra, Gozo, and its significance for the Neolithic sequence of Malta. *Arch. Anth. Sci.* 11, 4251-4306. doi.org/10.1007/s12520-019-00790-y

McLaughlin, R., Parkinson, E.W., Reimer, P.J., Malone, C. (2020a), "Dating Maltese Prehistory", in *Temple Places: Excavating cultural sustainability in prehistoric Malta*, eds. C. Malone, R. Grima, R. McLaughlin, E.W. Parkinson, S. Stoddart, N. Vella (Cambridge, McDonald Institute for Archaeological Research) 27-38.

Noti, R., van Leewen, J.F.N., Clombaroli, D., Vescovi, E., Pasta, S., La Mantia, T., et al. (2009). Mid- and late-Holocene vegetation and fire history at Biviere di Gela, a coastal lake in southern Italy. *Veg. Hist. Bot*. 18, 371-287. DOI: 10.1007/s00334-009-0211-0

Roberts, N., Woodbridge, J., Palmisano, A., Bevan, A., Fyfe, R., Shennan, S. (2019). Mediterranean landscape change during the Holocene: Synthesis, comparison and regional trends in population, land cover and climate. *The Holocene* 29, 923-937. https://doi.org/10.1177/0959683619826697

Stewart, M., Carleton, W.C., Groucutt, H.S. (2021). Climate change, not human population growth, correlates with Late Quaternary megafauna declines in North America. *Nat. Coms.* 12, 965. | https://doi.org/10.1038/s41467-021-21201-8 |

Tinner, W., van Leeuwen, J.F.N., Colombaroli, D., Vescovi, E., van der Knaap, W.O., Henne, P.D., Pasta, S., D'Angelo, S., La Mantia, T. (2009). Holocene environmental and climatic changes at Gorgo Basso, a coastal lake in southern Sicily, Italy. *Quatern. Sci. Rev.* 28, 1498-1510. doi:10.1016/j.quascirev.2009.02.001

Zanchetta, G., Regattieri, E., Isola, I., Drysdale, R. N., Bini, M., et al. (2016). The so-called "4.2 event" in the central Mediterranean and its climatic teleconnections. *Alpine and Quaternary* 29, 5-17.

R packages:

Michael J. Kane, John Emerson, Stephen Weston (2013). Scalable Strategies for Computing with Massive Data. Journal of Statistical Software, 55(14), 1-19. URL http://www.jstatsoft.org/v55/i14/.

H. Wickham. ggplot2: Elegant Graphics for Data Analysis. Springer-Verlag New York, 2016.

Alboukadel Kassambara (2020). ggpubr: 'ggplot2' Based Publication Ready Plots. R package version 0.4.0. https://CRAN.R-project.org/package=ggpubr

R Core Team (2021). R: A language and environment for statistical computing. R Foundation for Statistical Computing, Vienna, Austria. URL https://www.R-project.org/.

Supplementary Tables

Site	Laboratory number	Radiocarbon age (BP)	Error	Reference
Xaghra	OxA-3750	3580	75	Malone et al. (2019)
Xaghra	UBA-32019	3842	28	Malone et al. (2019)
Xaghra	UBA-32036	3846	33	Malone et al. (2019)
Xaghra	UBA-32014	3849	26	Malone et al. (2019)
Xaghra	UBA-32033	3857	36	Malone et al. (2019)
Xaghra	UBA-32043	3877	32	Malone et al. (2019)
Xaghra	UBA-32027	3893	28	Malone et al. (2019)
Xaghra	UBA-32015	3903	31	Malone et al. (2019)
Xaghra	UBA-32017	4009	39	Malone et al. (2019)
Xaghra	UBA-32018	3904	30	Malone et al. (2019)
Xaghra	SUERC-45309	3898	45	Malone et al. (2019)
Xaghra	SUERC-45310	3910	45	Malone et al. (2019)
Xaghra	SUERC-45312	3871	45	Malone et al. (2019)
Xaghra	SUERC-45311	3929	45	Malone et al. (2019)
Xaghra	SUERC-4391	3910	40	Malone et al. (2019)
Xaghra	SUERC-4390	3920	35	Malone et al. (2019)
Xaghra	UBA-32045	3926	28	Malone et al. (2019)
Xaghra	SUERC-45318	3941	45	Malone et al. (2019)
Xaghra	UBA-32020	3942	28	Malone et al. (2019)
Xaghra	OxA-27687	3942	28	Malone et al. (2019)

Xagħra	OxA-27840	3945	27	Malone et al. (2019)
Xagħra	UBA-32022	3947	32	Malone et al. (2019)
Xagħra	UBA-32062	3952	55	Malone et al. (2019)
Xagħra	UBA-32023	3955	31	Malone et al. (2019)
Xagħra	SUERC-45316	3957	45	Malone et al. (2019)
Xagħra	OxA-27838	3958	24	Malone et al. (2019)
Xagħra	UBA-32051	3963	32	Malone et al. (2019)
Xagħra	UBA-32053	3970	25	Malone et al. (2019)
Xagħra	UBA-32032	3983	48	Malone et al. (2019)
Xagħra	UBA-32034	3986	34	Malone et al. (2019)
Xagħra	UBA-32052	3987	27	Malone et al. (2019)
Xagħra	OxA-27839	3990	25	Malone et al. (2019)
Xagħra	SUERC-45317	4002	45	Malone et al. (2019)
Xagħra	UBA-32016	4017	31	Malone et al. (2019)
Xagħra	UBA-32044	4023	26	Malone et al. (2019)
Xagħra	OxA-27803	4027	26	Malone et al. (2019)
Xagħra	UBA-32037	4031	36	Malone et al. (2019)
Xagħra	UBA-32009	4032	31	Malone et al. (2019)
Xagħra	UBA-32012	4033	27	Malone et al. (2019)
Xagħra	SUERC-4389	4035	35	Malone et al. (2019)
Xagħra	UBA-32057	4036	27	Malone et al. (2019)
Xagħra	UBA-32060	4039	29	Malone et al. (2019)
Xagħra	OxA-33926	4040	35	Malone et al. (2019)
Xagħra	UBA-32024	4043	27	Malone et al. (2019)

Xagħra	UBA-32042	4047	32	Malone et al. (2019)
Xagħra	UBA-32039	4047	39	Malone et al. (2019)
Xagħra	UBA-10378	4048	28	Malone et al. (2019)
Xagħra	UBA-32031	4048	40	Malone et al. (2019)
Xagħra	OxA-33927	4050	36	Malone et al. (2019)
Xagħra	UBA-10383	4054	24	Malone et al. (2019)
Xagħra	OxA-27836	4058	26	Malone et al. (2019)
Xagħra	UBA-32049	4065	26	Malone et al. (2019)
Xagħra	UBA-32025	4066	27	Malone et al. (2019)
Xagħra	UBA-32021	4069	33	Malone et al. (2019)
Xagħra	OxA-27832	4077	33	Malone et al. (2019)
Xagħra	OxA-3571	4080	65	Malone et al. (2019)
Xagħra	OxA-33928	4096	36	Malone et al. (2019)
Xagħra	UBA-32056	4099	27	Malone et al. (2019)
Xagħra	UBA-32006	4102	30	Malone et al. (2019)
Xagħra	UBA-32048	4107	37	Malone et al. (2019)
Xagħra	UBA-32030	4109	34	Malone et al. (2019)
Xagħra	OxA-33924	4114	37	Malone et al. (2019)
Xagħra	UBA-32028	4118	33	Malone et al. (2019)
Xagħra	UBA-32059	4128	29	Malone et al. (2019)
Xagħra	UBA-32035	4129	39	Malone et al. (2019)
Xagħra	UBA-32050	4130	33	Malone et al. (2019)
Xagħra	UBA-32047	4131	25	Malone et al. (2019)

Xagħra	UBA-32013	4131	29	Malone et al. (2019)
Xagħra	UBA-32061	4133	41	Malone et al. (2019)
Xagħra	UBA-32008	4136	30	Malone et al. (2019)
Xagħra	UBA-32010	4147	31	Malone et al. (2019)
Xagħra	UBA-32041	4150	45	Malone et al. (2019)
Xagħra	UBA-32038	4162	35	Malone et al. (2019)
Xagħra	OxA-3573	4170	65	Malone et al. (2019)
Xagħra	UBA-32007	4184	33	Malone et al. (2019)
Xagħra	OxA-27834	4191	25	Malone et al. (2019)
Xagħra	OxA-33923	4194	37	Malone et al. (2019)
Xagħra	OxA-27837	4198	26	Malone et al. (2019)
Xagħra	UBA-32040	4208	73	Malone et al. (2019)
Xagħra	UBA-32011	4215	31	Malone et al. (2019)
Xagħra	OxA-27833	4219	26	Malone et al. (2019)
Xagħra	OxA-3575	4225	70	Malone et al. (2019)
Xagħra	OxA-33925	4234	35	Malone et al. (2019)
Xagħra	UBA-32026	4237	30	Malone et al. (2019)
Xagħra	OxA-3569	4250	65	Malone et al. (2019)
Xagħra	OxA-3574	4260	60	Malone et al. (2019)
Xagħra	UBA-32003	4263	33	Malone et al. (2019)
Xagħra	OxA-3570	4300	60	Malone et al. (2019)
Xagħra	UBA-32046	4351	29	Malone et al. (2019)
Xagħra	OxA-33922	4495	35	Malone et al. (2019)
Xagħra	OxA-33921	4554	37	Malone et al. (2019)

Xagħra	OxA-3566	4600	65	Malone et al. (2019)
Xagħra	UBA-32005	4727	52	Malone et al. (2019)
Xagħra	OxA-27802	4759	27	Malone et al. (2019)
Xagħra	OxA-3572	5380	70	Malone et al. (2019)
Bur Mgħeż	OxA-8165	4305	65	Malone et al (2009)
Ġgantija	UBA-33707	3962	50	McLaughlin et al (2020)
Ġgantija	UBA-35589	4106	35	McLaughlin et al (2020)
Ħal Saflieni	OxA-8197	4130	45	Malone et al (2009)
Kordin III	UBA-33017	4363	40	McLaughlin et al (2020)
Kordin III	UBA-33021	4391	34	McLaughlin et al (2020)
Kordin III	UBA-33023	4581	40	McLaughlin et al (2020)
Kordin III	UBA-33015	4593	31	McLaughlin et al (2020)
Kordin III	UBA-33018	4614	33	McLaughlin et al (2020)
Kordin III	UBA-37860	4628	34	McLaughlin et al (2020)
Kordin III	UBA-33016	4684	46	McLaughlin et al (2020)
Kordin III	UBA-37669	4693	31	McLaughlin et al (2020)
Kordin III	UBA-37665	4737	46	McLaughlin et al (2020)
Kordin III	UBA-33020	4741	45	McLaughlin et al (2020)
Qala il-Pellegrin	BM-808	3912	64	Fenech 2008
Santa Verna	UBA-33026	4324	31	McLaughlin et al (2020)
Santa Verna	UBA-31045	4491	52	McLaughlin et al (2020)
Santa Verna	UBA-37858	4491	43	McLaughlin et al (2020)
Santa Verna	UBA-33025	4500	33	McLaughlin et al (2020)

Santa Verna	UBA-31038	4501	34	McLaughlin et al (2020)
Santa Verna	UBA-31035	4525	35	McLaughlin et al (2020)
Santa Verna	UBA-31050	4636	43	McLaughlin et al (2020)
Santa Verna	UBA-31049	4664	41	McLaughlin et al (2020)
Santa Verna	UBA-31041	4908	37	McLaughlin et al (2020)
Santa Verna	UBA-33706	4945	87	McLaughlin et al (2020)
Skorba	BM-712	4478	56	Malone et al (2009)
Taċ-Ċawla	UBA-37864	3744	40	McLaughlin et al (2020)
Taċ-Ċawla	UBA-30423	3858	36	McLaughlin et al (2020)
Taċ-Ċawla	UBA-31711	3891	32	McLaughlin et al (2020)
Taċ-Ċawla	UBA-33027	3896	31	McLaughlin et al (2020)
Taċ-Ċawla	UBA-40322	3903	43	McLaughlin et al (2020)
Taċ-Ċawla	UBA-37683	3959	37	McLaughlin et al (2020)
Taċ-Ċawla	UBA-30422	4018	40	McLaughlin et al (2020)
Taċ-Ċawla	UBA-29835	4032	34	McLaughlin et al (2020)
Taċ-Ċawla	UBA-29836	4182	37	McLaughlin et al (2020)
Taċ-Ċawla	UBA-30416	4388	34	McLaughlin et al (2020)
Taċ-Ċawla	UBA-31713	4454	38	McLaughlin et al (2020)
Taċ-Ċawla	UBA-29833	4496	41	McLaughlin et al (2020)
Taċ-Ċawla	UBA-37863	4500	36	McLaughlin et al (2020)
Taċ-Ċawla	UBA-37866	4500	33	McLaughlin et al (2020)
Taċ-Ċawla	UBA-40320	4508	45	McLaughlin et al (2020)
Taċ-Ċawla	UBA-37862	4517	38	McLaughlin et al (2020)
Taċ-Ċawla	UBA-31714	4518	41	McLaughlin et al (2020)

Taċ-Ċawla	UBA-30418	4524	34	McLaughlin et al (2020)
Taċ-Ċawla	UBA-30417	4530	37	McLaughlin et al (2020)
Taċ-Ċawla	UBA-30419	4540	37	McLaughlin et al (2020)
Taċ-Ċawla	UBA-30414	4546	37	McLaughlin et al (2020)
Taċ-Ċawla	UBA-37681	4554	38	McLaughlin et al (2020)
Taċ-Ċawla	UBA-30413	4610	37	McLaughlin et al (2020)
Taċ-Ċawla	UBA-37865	4616	32	McLaughlin et al (2020)
Taċ-Ċawla	UBA-40321	4634	36	McLaughlin et al (2020)
Taċ-Ċawla	UBA-30420	4679	41	McLaughlin et al (2020)
Taċ-Ċawla	UBA-30421	4738	35	McLaughlin et al (2020)
Taċ-Ċawla	UBA-33028	4776	35	McLaughlin et al (2020)
Taċ-Ċawla	UBA-30415	4849	38	McLaughlin et al (2020)
Tarxien	BM-710	3286	72	Malone et al (2009)
Tarxien	BM-711	3354	76	Malone et al (2009)
Tarxien	UBA-35591	3479	30	McLaughlin et al (2020)
Tarxien	UBA-35592	3567	30	McLaughlin et al (2020)
Xemxija	UBA-35296	4068	46	McLaughlin et al (2020)
Xemxija	UBA-35298	4168	38	McLaughlin et al (2020)
Xemxija	UBA-35295	4177	36	McLaughlin et al (2020)
Xemxija	UBA-35297	4442	33	McLaughlin et al (2020)
Xemxija	UBA-35294	4602	31	McLaughlin et al (2020)

Supplementary table 1. Compilation of uncalibrated radiocarbon dates for Maltese islands for period 3500 to 2730 cal. BC.

Value	Whole sample (n=35)	Key contexts (N=20)
Mean	137.3	137.3
Minimum	136.4	136.8
Maximum	137.8	137.6
25%	137.1	137.1
75%	137.4	137.4
Standard deviation	0.3	0.2

Supplementary table 2. Data on vertical distribution (m) of broken statue pieces at Xaghra Circle. The key contexts (514, 783, 931, 942) remove contexts where only one or two fragments were found

Model	Boundary 1	Boundary 2	A_model	A_overall	Span_95_L	Span_95_U	Notes
1	Boundary	Boundary	56.3	53.1	146	363	Discrete event with abrupt initiation and termination.
2	Sigma	Boundary	84.3	84.3	187	511	Some older dates included in an otherwise singular event with an abrupt termination.
3	Sigma	Sigma	83.9	80.5	205	530	Older and younger dates potentially included in the target deposition event, but concentrated around a central time.
4	Tau	Boundary	92.7	92.8	196	552	Gradual accumulation of samples included in a final, abruptly terminating deposition event with at least a few very old samples included.

Supplementary table 3. Summary of chronological models.

Supplementary Figures

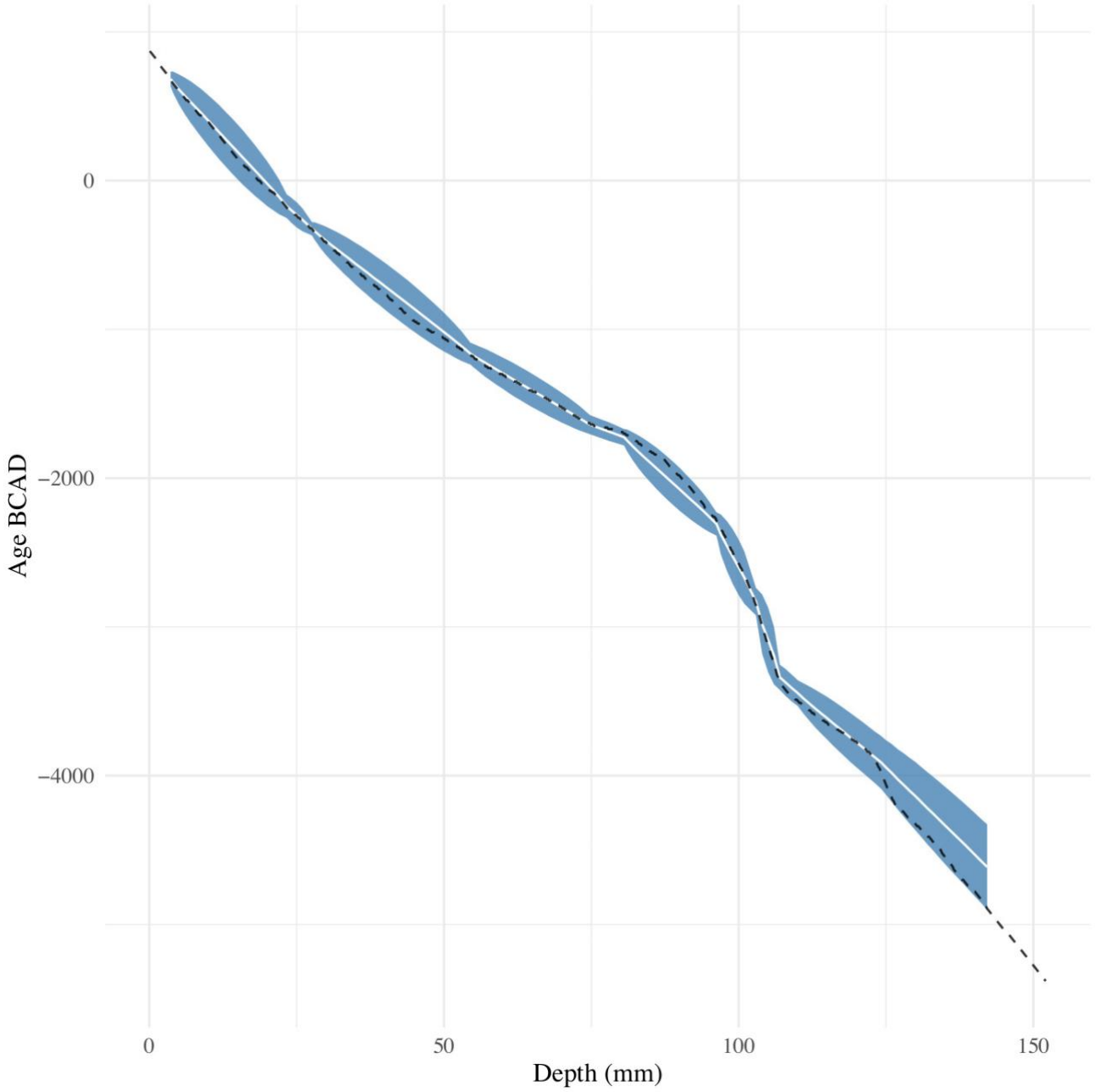

Supplementary Figure 1. Comparison of age-depth models for Renella Cave. The white line indicates the age-depth relationship according to OxCal's Poisson accumulation model and the steel-blue envelope indicates the 95% confidence interval for that model. The black dashed line is the published age-depth interpolation for the RL4 flowstone d18O record. The mean of the OxCal model we produced is very close to the published RL4 age-depth interpolation with the latter contained within the 95% confidence interval of the former.

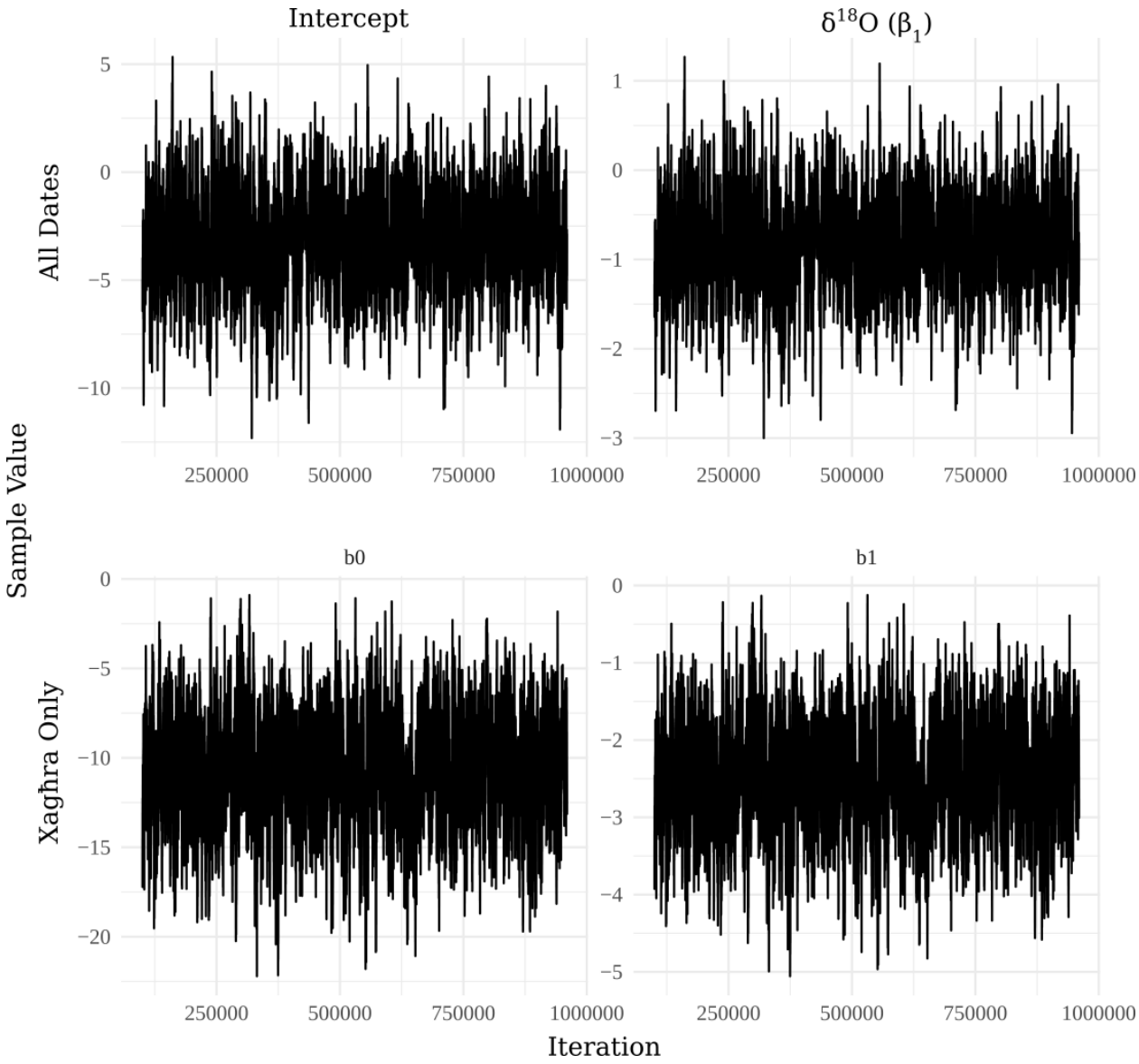

Supplementary figure 2. These plots show the MCMC chains for the two main regression parameters of the REC models we generated. The top row displays the chains for the analysis involving all C14 dates from Malta while the bottom row displays the chains for the analysis involving only dates from Xaghra circle. The left column contains the chains for the model intercepts (average C14 count when the d18O record is zero) and the right column contains the chains for the key regression coefficients pertaining to the d18O record.